,

Giant reversible rotating cryomagnetocaloric effect in $KEr(MoO_4)_2$ induced by a crystal-field anisotropy

V. Tkáč*
Institute of Physics, P. J. Šafárik University, Park Angelinum 9, 04001 Košice, Slovak Republic
and Department of Condensed Matter Physics, Faculty of Mathematics and Physics, Charles University in Prague, Ke Karlovu 5, 12116 Prague, Czech Republic

A. Orendáčová,† E. Čižmár, M. Orendáč, and A. Feher
Institute of Physics, P. J. Šafárik University, Park Angelinum 9, 04001 Košice, Slovak Republic

A. G. Anders
B. I. Verkin Institute for Low Temperature Physics and Engineering of NASU, Lenin Av. 47, 61103 Kharkov, Ukraine
(Received 28 May 2015; revised manuscript received 18 June 2015; published 7 July 2015)

Magnetocaloric properties of $KEr(MoO_4)_2$ single crystals were investigated using magnetization and specific heat measurements in the magnetic field applied along the easy and hard axis. Large conventional magnetocaloric effect was found around 10 K ($-\Delta S_{max} = 14$ J/kg K for 5 T) in the field applied along the easy axis. What is more, a huge magnetic anisotropy in the *ab* plane leads to a large anisotropy of magnetocaloric effect, $-\Delta S_{R,max} = 10$ and 13 J/kg K obtained by a simple rotating of the single crystal within the *ab* plane in the constant magnetic field 2 and 5 T, respectively. Large ΔS_R values with no hysteresis losses and rather wide working temperature spans imply that $KEr(MoO_4)_2$ may serve as a promising candidate for the implementation of a compact rotary magnetic cryorefrigerator.

DOI: 10.1103/PhysRevB.92.024406 PACS number(s): 75.30.Sg, 71.70.Ch, 75.30.Gw, 76.30.Kg

I. INTRODUCTION

Magnetic cooling based on magnetocaloric effect (MCE) in solids becomes more important due to higher efficiency and the use of environmentally friendly materials [1,2]. Giant MCE reported for a broad variety of materials is usually associated with a phase transition of the first order (FO) and involves a significant latent heat. However, a hysteresis accompanying the transition, reduces the refrigerant's capacity [3]. Another problem is a slow kinetics of the FO transition, limiting the adiabatic changes of temperature, ΔT_{ad}, since magnetic refrigerators operate between 0.1 and 4 Hz and much MCE will be lost during variation of magnetic field [3]. In the systems with second-order (SO) magnetic phase transition, the largest MCE is expected when the heat capacity of the material is strongly affected by the magnetic field [4]. In both cases the maximum MCE occurs in the vicinity of the SO (FO) phase transition, thus, the control of magnetic ordering is important for certain applications.

While at high temperatures, the large lattice specific heat leads to the increase of the thermal load of the refrigerant itself, at low temperatures the lattice contribution diminishes. Correspondingly, besides the systems with magnetic phase transition [5,6], more options are available for magnetic cryocooling. More specifically, paramagnets under special conditions enhancing MCE, namely geometrically frustrated magnets in the vicinity of the saturation field [7,8], in the region close to a field-induced quantum-critical point [9], molecular magnets [10], paramagnets containing high spin ions with vanishing magnetic anisotropy [11], etc. All these examples of MCE require varying magnetic field between zero and some rather high value, typically 7–8 T.

Anisotropic MCE is another alternative, obtained simply by rotating a single crystal in a constant magnetic field. A theoretical study derived anisotropic MCE in Laves phase compounds considering the Hamiltonian with crystal-field and quadrupolar effects taken account in addition to magnetoelastic coupling and exchange interactions [12]. The authors showed that in some cases the use of anisotropic materials can significantly increase the cooling capacity. Anisotropic MCE resulting from the anisotropic behavior in the magnetic ordered phase was systematically investigated in the series $RMnO_3$ (R = Dy, Tb, Ho, Yb). A maximal "rotated" magnetic entropy change $-\Delta S_{R,max} \approx 11.5$ J/kg K was observed in Dy and Tb compounds at temperatures about 10 K and magnetic field 5 T, produced by the rotation of the magnetic field vector between the easy and hard axis of magnetization [13,14]. A comparable anisotropy of MCE ($-\Delta S_{R,max} \approx 12.4$ J/kg K) was observed in a magnetic insulator $HoMn_2O_5$ around 10 K in the field 7 T and was attributed to a combined effect of a large magnetocrystalline anisotropy and complexity of magnetic interactions resulting in the magnetic ordering of Ho^{3+} moments [15]. A huge anisotropy of MCE has been recently reported for conducting material PrSi in the vicinity of the first-order-like magnetic phase transition with $T_C = 52$ K. Application of magnetic field from 0 to 7 T along the [010] and [100] axis produced entropy change $-\Delta S_M \approx 22$ J/kg K and -0.4 J/kg K, respectively [16].

While anisotropic MCE reported in literature was observed as a result of the combined effect of magnetocrystalline anisotropy and SO (FO) magnetic phase transition, the present work is devoted to the investigation of the anisotropic MCE in a paramagnet with a large easy-axis anisotropy introduced by

*vladimir.tkac@mag.mff.cuni.cz
†alzbeta.orendacova@upjs.sk

a crystal field. The study of anisotropic MCE is performed in a single crystal of $KEr(MoO_4)_2$. The compound is an insulator. The first coordination sphere of the Er^{3+} ion consists of eight oxygen atoms forming a slightly distorted square antiprism. The ground state of a free Er^{3+} is $^4I_{15/2}$ multiplet, which is split into eight Kramers doublets with the energies $E/k_B = 22$, 46, 107, 266, 372, 456, and 467 K above the ground doublet [17]. Electron paramagnetic resonance spectra [18] and isothermal magnetization [19] measured above 2 K revealed a strong anisotropy of a ground doublet characterized by anisotropic g-factor values 19, 2, and 0.7, measured along the easy, medium, and hard magnetization axis, respectively. Relatively weak spin-phonon coupling influences the position of the first excited doublet due to interaction of the electronic state with the transverse acoustic vibration modes. The study of diluted samples [18] revealed that in the absence of the coupling, the energy of the doublet reduces to 11.5 K. Previous thermodynamic studies of a concentrated compound [20,21] indicated a presence of magnetic correlations which can be described by a model of a two-dimensional array of $S = 1/2$ ferromagnetic Ising chains with an intrachain coupling, $|J_1|/k_B \approx 0.85$ K and an interchain antiferromagnetic coupling, $|J_2| \approx 0.2\,|J_1|$. Long-range magnetic ordering of Er^{3+} moments in zero magnetic field was observed at $T_C = 0.95$ K. The magnetic order is very fragile since already small magnetic field $B \approx 100$ mT applied along the easy axis completely suppressed a phase transition [21].

Thus, the investigation of MCE in $KEr(MoO_4)_2$ at temperatures above 2 K excludes any possibility of the interplay between magnetic phase transition and crystal-field anisotropy.

II. EXPERIMENTAL DETAILS

Single crystals of $KEr(MoO_4)_2$ were synthesized using conventional solid-state reactions with starting materials Er_2O_3, MoO_3, K_2SO_4, and Al_2O_3. More details about sample preparation can be found in Refs. [22,23]. The system crystallizes in the orthorhombic structure, $Pbcn$ (D_{2h}^{14}) space group, with 4 f.u. in the cell and lattice parameters $a = 5.063$ Å, $b = 18.25$ Å, and $c = 7.917$ Å. Crystals grow in the form of thin plates parallel to ac layers with a pronounced lamination within the [010] cleavage plane as a result of very weak coupling between the layers along the b axis. A commercial Quantum Design SQUID magnetometer was used for the study of isothermal magnetization curves investigated in the temperature range nominally from 2 to 60 K in magnetic fields B ($=\mu_0 H$) up to 5 T. Single crystals with a mass of 27.2 mg and 11.7 mg were used for magnetic measurements in $B \parallel a$ and $B \parallel b$, respectively. Specific heat of a single crystal with a mass of 1 mg was investigated at temperatures varying from 2 to 50 K in zero magnetic field in a commercial Quantum Design PPMS device.

III. RESULTS AND DISCUSSION

Isothermal magnetization curves in the magnetic field applied along the crystallographic axis a (easy axis) and axis b (hard axis) are shown in Fig. 1. Since no hysteresis was observed at these temperatures and magnetic fields, a reversible MCE can be expected. In the field applied along the easy axis, a magnetization achieves a saturation already in 1 T

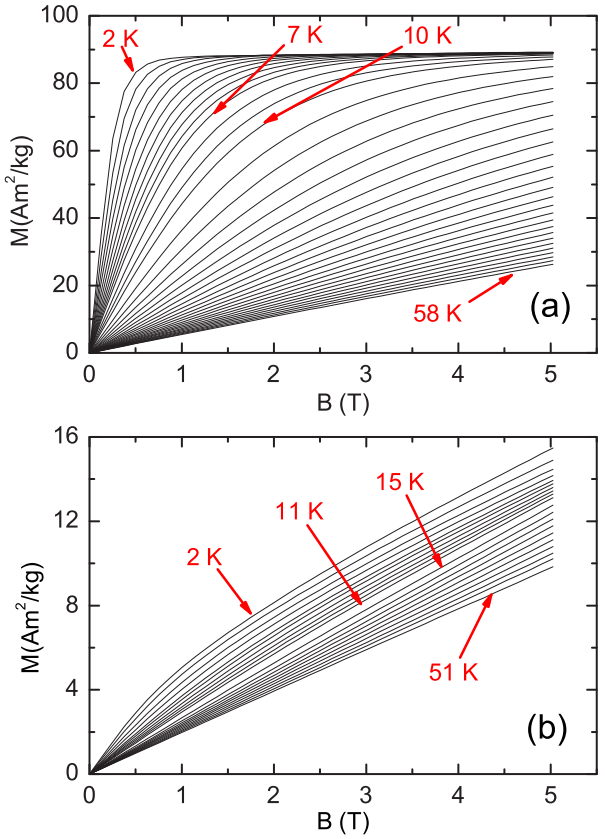

FIG. 1. (Color online) Isothermal magnetization curves of $KEr(MoO_4)_2$ for (a) $B \parallel a$, temperature step $\Delta T = 0.5$, 1, and 2 K for the interval 2–7, 7–10, and 10–58 K, respectively. (b) $B \parallel b$, $\Delta T = 1$ and 4 K for the interval 2–11 and 11–51 K, respectively.

at helium temperatures. The change of magnetic field direction from the a to b axis at 2 K leads to about 95% reduction of magnetization in the field of 1 T.

In the first approximation, the magnetic behavior can be described using the Hamiltonian,

$$H = H_{CEF} + H_{MAG} \tag{1}$$

considering only crystal electric field (CEF) and magnetic field effects. The Zeeman term is of the form $H_{MAG} = g_J \mu_B J B$, where g_J, μ_B, and J stands for the Landé factor, Bohr magneton, and total angular momentum, respectively. $H_{CEF} = \sum_{q=0}^{2} A_2^q \langle r^2 \rangle \alpha O_2^q + \sum_{q=0}^{4} A_4^q \langle r^4 \rangle \beta O_4^q + \sum_{q=0}^{6} A_6^q \langle r^2 \rangle \gamma O_6^q$ is expressed in Abragam and Bleaney notation [24]. O_k^q represents equivalent operators, the coefficients α, β, and γ are the constants tabulated by Stevens [25] and $A_k^q \langle r^k \rangle$ are crystal-field parameters. Since the local symmetry of the Er^{3+} site is quite low (C_2), 15 parameters are required. This simplified approach neglects a presence of a weak spin-phonon coupling which can potentially affect the values of CEF parameters given in Table I. The parameters were obtained by the analysis of magnetization curves for $B \parallel a$ within a model [Eq. (1)]. A corresponding energy spectrum was calculated, reflecting the main features of experimental spectra [18] in $B \parallel a$ (Fig. 2). A good agreement achieved between theoretical and experimental data indicates that in this

TABLE I. Effective CEF parameters obtained from the analysis of magnetization curves in $B \parallel a$ (in units of Kelvin).

$A_2^0\langle r^2\rangle$	$A_2^1\langle r^2\rangle$	$A_2^2\langle r^2\rangle$	$A_4^0\langle r^4\rangle$	$A_4^1\langle r^4\rangle$
−153.7	568.8	−114.0	77.4	493.1
$A_4^2\langle r^4\rangle$	$A_4^3\langle r^4\rangle$	$A_4^4\langle r^4\rangle$	$A_6^0\langle r^6\rangle$	$A_6^1\langle r^6\rangle$
188.1	−1310.9	982.4	−29.5	604.2
$A_6^2\langle r^6\rangle$	$A_6^3\langle r^6\rangle$	$A_6^4\langle r^6\rangle$	$A_6^5\langle r^6\rangle$	$A_6^6\langle r^6\rangle$
−11.3	0.7	−165.0	−433.9	−0.1

orientation, a crystal field is a main mechanism controlling thermodynamic properties at temperatures above 2 K. The same approach applied in the analysis of magnetization data in the orientation $B \parallel b$ did not yield satisfying results, probably, due to a reinforced influence of the spin-phonon coupling in a transversal magnetic field.

The isothermal magnetic entropy change ΔS_M has been calculated using the Maxwell relation [3],

$$\Delta S_M(T,\Delta B) = \int_{B_i}^{B_f} \frac{\partial M(T,B)}{\partial T} dB, \qquad (2)$$

where B_i and B_f represent initial and final magnetic field. Temperature dependence of $-\Delta S_M$ derived from experimental magnetization data for $B_i = 0$ and several values of B_f applied along the a and b axes is shown in Fig. 3. For comparison, we also calculated theoretical magnetizations and corresponding $-\Delta S_M$ values from CEF parameters for the same values of B_f applied along the a axis. We can see, that at low temperatures ($T < 2$ K), all theoretical $-\Delta S_M$ values merge with the entropy S_{CEF} derived from the simple model [Eq. (1)] in $B = 0$ T. A finite value of $S_{CEF}(B = 0)$ at low temperatures results from a double degeneracy of the CEF ground state (Fig. 2, inset). The removal of the rest entropy by internal magnetic fields arising from short-range magnetic correlations developing below 4 K, is reflected in the rapid decrease of a total (lattice and magnetic) entropy, $S_{C,TOT}$, calculated from the experimental specific heat in $B = 0$ T [Figs. 3(a) and 4(a), inset]. For the extrapolation to lowest temperatures, total

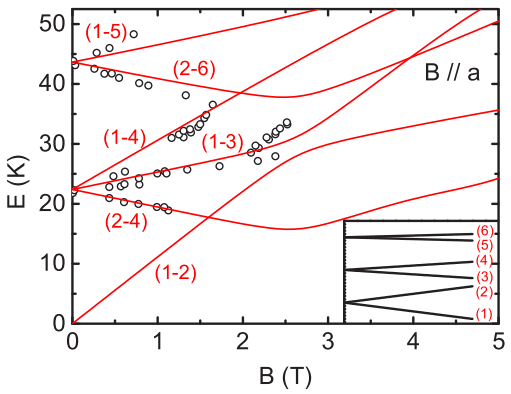

FIG. 2. (Color online) Field dependence of the transitions between energy levels in $B \parallel a$. Solid lines represent transitions generated from crystal field parameters given in Table I. The points represent the experimental data from Ref. [18]. The numbers denote transitions between energy levels (see inset).

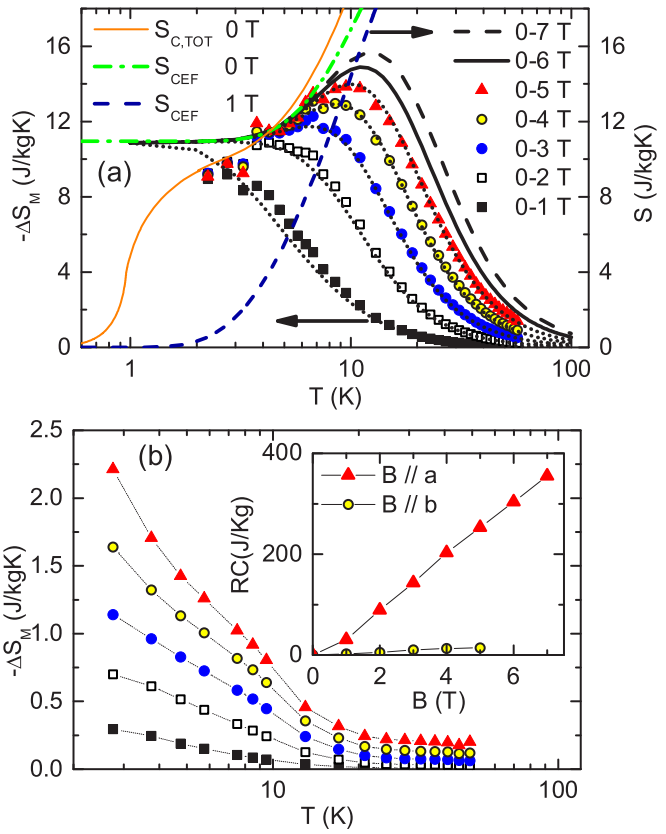

FIG. 3. (Color online) (a) (Left axis) Temperature dependence of the isothermal entropy change in $KEr(MoO_4)_2$ under different magnetic field, $B \parallel a$. Symbols represent $-\Delta S_M$ values obtained from experimental magnetization curves; lines represent $-\Delta S_M$ values calculated from magnetization curves derived from CEF parameters. (Right axis) Temperature dependence of the entropy (for more details, see text). (b) Temperature dependence of the isothermal entropy change in $KEr(MoO_4)_2$ in $B \parallel b$. Symbols have the same meaning as in (a); lines are only guides for the eyes. (Inset) Field dependence of the refrigerant capacity. The RC values for a field above 5 T are derived from CEF parameters.

entropy data from Ref. [26] were used. It is evident, that below 10 K, CEF contribution dominates in a total entropy and a lattice entropy can be neglected. The application of external magnetic field leads to an exponential decrease of the $S_{CEF}(B)$ at lowest temperatures. As a consequence, S_{CEF} calculated for $B = 1$ T achieves nearly zero values at temperatures below 2 K [Fig. 3(a)]. Increasing magnetic field enforces the exponential decrease, shifting the region of nearly zero $S_{CEF}(B)$ values towards higher temperatures.

This result suggests, that all real $-\Delta S_M$ vs T dependencies should undergo a crossover between a low-temperature and a high-temperature regime. The former is characterized by a dominant contribution of internal magnetic fields to $-\Delta S_M$. As a consequence, at least for $B \geqslant 1$ T, $S_{C,TOT}(B = 0)$ vs T dependence forms an envelope of a low-temperature side of the experimental $-\Delta S_M$ maxima depicted in Fig. 3(a). Concerning higher temperatures, at least above 4 K, the contribution of the crystal field prevails in all studied magnetic fields, leading to large conventional magnetocaloric effect ($-\Delta S_{max} = 14$ J/kg K)

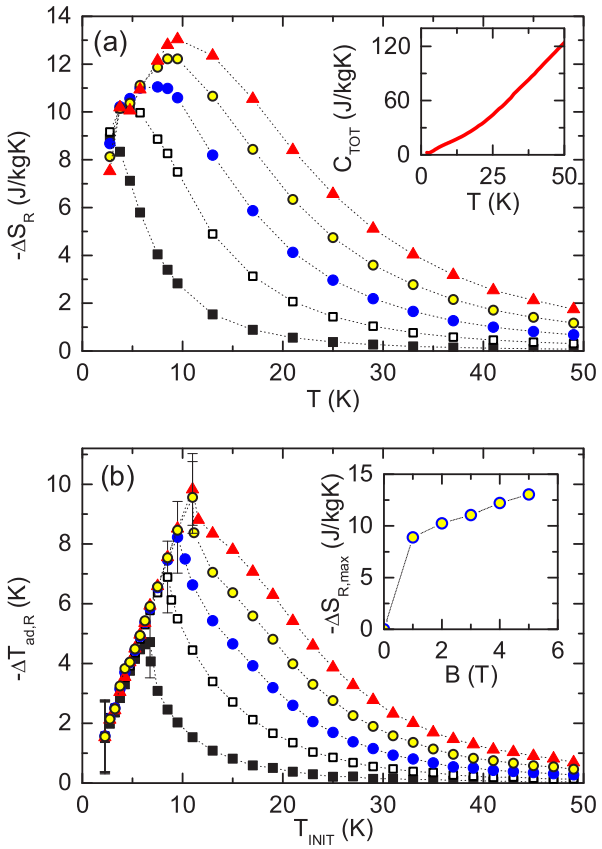

FIG. 4. (Color online) (a) Isothermal entropy changes related to a rotation of $KEr(MoO_4)_2$ single crystal between the a and b axes in constant magnetic fields 1 T (solid black square), 2 T (open square), 3 T (solid blue circle), 4 T (solid yellow circle), and 5 T (red triangle), applied initially along the b axis. (Inset) Temperature dependence of the specific heat in $B = 0$ T. (b) Adiabatic temperature change as a function of initial temperature in constant fields 1 T (solid black square), 2 T (open square), 3 T (solid blue circle), 4 T (solid yellow circle), and 5 T (red triangle), applied initially along the easy axis. (Inset) Field dependence of $-\Delta S_{R,max}$.

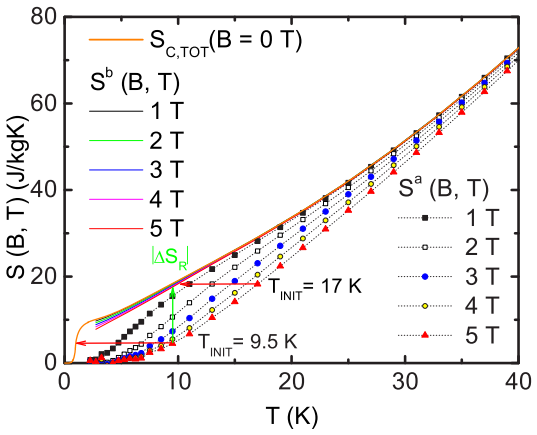

FIG. 5. (Color online) Temperature dependence of the entropy in $KEr(MoO_4)_2$. A thick line represents $S_{C,TOT}$, (magnetic and lattice contribution) calculated from the experimental specific heat in $B = 0$ T. Thin solid lines represent entropies in magnetic field applied along the b axis. Symbols correspond to entropies in magnetic field applied along the a axis, dotted lines are guides for eyes. The horizontal arrows show how much the sample is cooled in the isentropic process $(S^a(B = 5\text{ T}, T_{INIT})) = (S^b(B = 5\text{ T}, T_{FIN}))$, while a vertical arrow demonstrates an example of isothermal rotating entropy change $|\Delta S_R|$ in a constant magnetic field 5 T.

at temperatures around 10 K in the field 5 T, applied along the easy axis.

Concerning the isothermal entropy change in $B \parallel b$, as expected from magnetization data (Fig. 1), the values are much lower than those in the field applied along the easy axis and do not reach maximum values in the accessible temperature range (Fig. 3). Besides a magnetization and entropy change, the strong magnetocrystalline anisotropy introduces a strong anisotropy also into a refrigerant capacity (RC). The quantity was calculated from the experimental $-\Delta S_M$ values, using a relation $RC = \int_{T_{cold}}^{T_{hot}} \Delta S_M(T)dT$, where T_{cold} and T_{hot} denote a working temperature interval of the refrigerant [3] (Fig. 3, inset). We used $T_{cold} = 2$ K, while T_{hot} is a temperature, at which the quantity $-\Delta S_M$ reaches half of the maximum value. In the field applied along the easy a axis, the value of RC is 253 J/kg for 5 T, whereas for the same field applied along the b axis, it is only 15 J/kg. The values are rather underestimated due to a choice of T_{cold}. For comparison with other refrigerants, recently reported RC of $HoMn_2O_5$ and Ho_2CoGa_3 was 210 J/kg and 287 J/kg for 5 T [5,15]. It should be noted, that unlike $HoMn_2O_5$, Ho_2CoGa_3, and other MCE materials [5], the magnetocrystalline anisotropy in $KEr(MoO_4)_2$ introduces large entropy changes already in relatively weak magnetic fields applied along the easy axis, leading to enhanced RC values. As a result, for 2 T, RC is 90 J/kg, which is two times larger than that for $HoMn_2O_5$.

A giant anisotropy in the thermodynamic properties suggests a presence of a giant rotating MCE in $KEr(MoO_4)_2$. Previous studies [14,15] revealed that a contribution of magnetocrystalline anisotropy to rotating MCE can be simply expressed $\Delta S_R = \Delta S_M(\Theta) - \Delta S_M(90^\circ)$, where Θ is an angle between the easy axis and magnetic field, $\Theta = 90^\circ$ corresponds to magnetic field applied along the hard magnetization axis, and ΔS_R represents a resulting isothermal rotating entropy change. Thus, considering the initial sample position in magnetic field applied along the hard axis, $B \parallel b$, after the isothermal rotation of a sample by 90° in a constant field achieving final orientation along the easy axis, $B \parallel a$, the resulting isothermal rotating entropy change can be expressed $\Delta S_R = \Delta S_M(B \parallel a)$-$\Delta S_M(B \parallel b)$. The results are depicted in Fig. 4(a). As can be seen, a maximal $-\Delta S_R$ value in the field 5 T is 13 J/kgK, while for $HoMn_2O_5$, a value 10 J/kgK was reported [15]. What is more, even in the field 2 T and temperature 4 K, there is still a large value, $-\Delta S_R = 10$ J/kgK pointing at the effectiveness of rotating MCE in $KEr(MoO_4)_2$ at rather low magnetic field [Fig. 4(b), inset]. The adiabatic temperature change associated with a rotation of a sample in constant magnetic field in adiabatic conditions, $-\Delta T_{ad,R}$, is shown in Fig. 4(b). The procedure of determination of $-\Delta T_{ad,R}$, when the sample is rotated from the orientation $B \parallel a$ to $B \parallel b$ is depicted in Fig. 5.

The entropy curves $S(B,T)$ for each field B, and temperature T, were obtained using a relation $S^a(B,T) = S_{C,TOT}(B = 0,T)$-$|\Delta S_M(B \parallel a,T)|$ and

$S^b(B,T) = S_{C,TOT}(B = 0,T)$-$|\Delta S_M(B \parallel b,T)|$. The expressions $|\Delta S_M(B \parallel a,T)|$ and $|\Delta S_M(B \parallel b,T)|$ denote absolute values of isothermal entropy changes in $B \parallel a$ and $B \parallel b$, respectively, depicted together with $S_{C,TOT}(B = 0,T)$ in Fig. 3. As can be seen from Fig. 5, the lack of magnetization data and corresponding $-\Delta S_M$ values below 2 K for fields applied along the (hard) b axis prevented us from the evaluation of $-\Delta T_{ad,R}$ for initial temperatures lower than some limiting value, e.g., for field $B = 5$ T, the limiting temperature is about 11 K. Since isothermal entropy change $|\Delta S_M(B \parallel b,T)|$ is very small, an approximation, $S^b(B,T) \approx S_{C,TOT}(B = 0,T)$, was used for the extrapolation of $S^b(B,T)$ curves far below 2 K (Fig. 5). Potential uncertainties in the determination of adiabatic temperature change, introduced by such approximation, can be in the order of 1 K and are denoted by error bars in Fig. 4(b). For clarity, for each magnetic field, the error bars are involved only for those $-\Delta T_{ad,R}$ values which correspond to the highest and lowest initial temperatures, all lower than the limiting temperature, mentioned above. The resulting dependencies, $-\Delta T_{ad,R}$ vs initial temperature, are characterized by a maximum, standardly shifting to lower temperatures in lower fields [15]. Apparently, the rotation of a crystal from the a to b axis in the field 5 T at an initial temperature 11.5 K [the lowest temperature which does not require extrapolation of $S^b(B,T)$ curves], leads to $-\Delta T_{ad,R} \approx 9$ K, which is sufficient for a cooling process [15].

IV. CONCLUSIONS

In conclusion, we studied magnetocaloric properties of the single crystal $KEr(MoO_4)_2$. The giant anisotropic MCE can be associated predominantly with CEF effects. The maximum value of the isothermal entropy change in the field 5 T applied along the easy axis is about 14 J/kgK, with a refrigerant capacity of 253 J/kg. A rotation of a crystal between a hard and easy axis in the magnetic field 5 T, is associated with the maximal entropy change $|\Delta S_R| \approx 13$ J/kgK at helium temperatures. Correspondingly, the studied compound can be used as a cryorefrigerant in two ways: rotating in constant magnetic fields and in varying magnetic fields applied along the easy axis. The absence of thermal hysteresis, field hysteresis losses, as well as a chemical stability makes the $KEr(MoO_4)_2$ single crystals highly attractive for magnetic refrigeration at low temperatures.

ACKNOWLEDGMENTS

This work has been supported by VEGA Grant No. 1/0143/13, Projects No. APVV-0132-11, No. 0014-11, and No. 14-0073, and ERDF EU Project No. ITMS26220120005. Financial support from US Steel DZ Energetika is greatly acknowledged.

[1] A. M. Tishin and Y. I. Spichkin, *The Magnetocaloric Effect and its Applications* (Institute of Physics Publishing, Bristol, Philadelphia, 2003).
[2] O. Tegus, E. Brück, K. H. J. Buschow, and F. R. de Boer, Nature (London) **415**, 150 (2002).
[3] K. A. Gschneidner, Jr., V. K. Pecharsky, and A. O. Tsokol, Rep. Prog. Phys. **68**, 1479 (2005).
[4] V. K. Pecharsky, K. A. Gschneidner, Jr., A. O. Pecharsky, and A. M. Tishin, Phys. Rev. B **64**, 144406 (2001).
[5] L. C. Wang, L. Cui, Q. Y. Dong, Z. J. Mo, Z. Y. Xu, F. X. Hu, J. R. Sun, and B. G. Shen, J. Appl. Phys. **115**, 233913 (2014).
[6] B. Emre, S. Yüce, E. Stern-Taulats, A. Planes, S. Fabbrici, F. Albertini, and L. Mañosa, J. Appl. Phys. **113**, 213905 (2013).
[7] M. E. Zhitomirsky, Phys. Rev. B **67**, 104421 (2003).
[8] O. Derzhko, J. Richter, O. Krupnitska, and T. Krokhmalskii, Phys. Rev. B **88**, 094426 (2013).
[9] L. Zhu, M. Garst, A. Rosch, and Q. Si, Phys. Rev. Lett. **91**, 066404 (2003).
[10] M. Evangelisti, A. Candini, M. Affronte, E. Pasca, L. J. de Jongh, R. T. W. Scott, and E. K. Brechin, Phys. Rev. B **79**, 104414 (2009).
[11] Y.-C. Chen, L. Quin, Z.-S. Meng, D.-F. Yang, Ch. Wu, Z. Fu, Y.-Z. Zheng, J.-L. Liu, R. Tarasenko, M. Orendáč, J. Prokleška, V. Sechovský, and M.-L. Tong, J. Mater. Chem. A **2**, 9851 (2014).
[12] A. L. Lima, K. A. Gschneidner, Jr., and V. K. Pecharsky, J. Appl. Phys. **96**, 2164 (2004).
[13] A. Midya, S. N. Das, P. Mandal, S. Pandya, and V. Ganesan, Phys. Rev. B **84**, 235127 (2011).
[14] J.-L. Jin, X.-Q. Zhang, G.-K. Li, Z.-H. Cheng, L. Zheng, and Y. Lu, Phys. Rev. B **83**, 184431 (2011).
[15] M. Balli, S. Jandl, P. Fournier, and M. M. Gospodinov, Appl. Phys. Lett. **104**, 232402 (2014).
[16] P. K. Das, A. Bhattacharyya, R. Kulkarni, S. K. Dhar, and A. Thamizhavel, Phys. Rev. B **89**, 134418 (2014).
[17] A. A. Loginov, Low Temp. Phys. **28**, 755 (2002).
[18] V. I. Kuťko, Low Temp. Phys. **31**, 1 (2005).
[19] S. Maťaš, E. Dudzik, R. Feyerherm, S. Gerischer, S. Klemke, K. Prokeš, and A. Orendáčová, Phys. Rev. B **82**, 184427 (2010).
[20] A. Orendáčová, M. Orendáč, V. Bondarenko, A. Feher, and A. G. Anders, J. Phys.: Condens. Matter **10**, 1125 (1998).
[21] A. Orendáčová, D. Horváth, M. Orendáč, E. Čižmár, M. Kačmár, V. Bondarenko, A. G. Anders, and A. Feher, Phys. Rev. B **65**, 014420 (2001).
[22] V. A. Vinokurov and P. V. Klevtsov, Kristallografiya **17**, 127 (1972).
[23] B. M. Wanklyn and F. R. Wondre, J. Cryst. Growth **43**, 93 (1978).
[24] A. Abragam and B. Bleaney, *Electron Paramagnetic Resonance* (Clarendon Press, Oxford, 1970).
[25] K. W. H. Stevensr, Proc. Phys. Soc. A **65**, 209 (1952).
[26] J. Hanko, M. Orendáč, M. Kajňaková, A. Orendáčová, and A. Feher, A. Phys. Pol. A **113**, 465 (2008).